Mechanics of Materials 134 (2019) 143–152

Contents lists available at ScienceDirect

Mechanics of Materials

journal homepage: www.elsevier.com/locate/mechmat

Research paper

Extraction of superelasticity parameter values from instrumented indentation via iterative FEM modelling

FF Roberto-Pereira, JE Campbell, J Dean, TW Clyne*

Department of Materials Science & Metallurgy, Cambridge University, 27 Charles Babbage Road, Cambridge CB3 0FS, UK

ARTICLE INFO

Keywords:
Indentation
Superelasticity
Finite element analysis

ABSTRACT

This paper concerns the use of (load-displacement) data obtained during spherical indentation of a superelastic (NiTi) alloy, so as to obtain a stress-strain curve. The methodology, which is already starting to become established for conventional plasticity, involves iterative FEM simulation of the indentation process, aiming to optimize agreement between modeled and measured outcomes (load-displacement plots in this case), by systematically varying the values of the parameters in a constitutive law. This worked well for the loading part of the stress-strain curve, but much more poorly for the unloading part. This inaccuracy is attributed to limitations in the standard representation (as implemented via the UMAT routine in ABAQUS) of the unloading part of the loop. A simple analytical formulation is proposed that might be suitable for future use in FEM software for simulation of superelastic deformation.

1. Introduction

Shape memory alloys (SMAs) continue to be subjected to intensive study and development. The most common SMA system is nickel-titanium, usually with a composition close to Ni-50 at%Ti (Saburi, 1998; Van Humbeeck and Stalmans, 2002; Van Humbeeck, 2001; Otsuka and Ren, 2005). Below M_f, defined as the temperature at which (shear) transformation of the parent austenitic phase to the martensitic phase is complete, the latter (monoclinic B19' structure in the Ni-Ti case) is thermodynamically stable. On heating to a higher temperature A_f, reversion to the parent phase (cubic B2 structure in the Ni-Ti case) is complete. Above A_f, SMAs can demonstrate superelasticity (SE), in which large mechanically-imposed strains (up to ~ 8%) can be accommodated by transformation of the parent phase to metastable martensitic variants. These variants revert to the parent phase on removal of the applied load. The shape memory effect (SME) can also be observed in these alloys. Application of stress at a temperature below M_f can lead to the strain being accommodated by reorientation of martensitic variants. On heating above A_f, however, the martensite can transform to the parent phase in such a way that the original shape is recovered. Subsequent (unloaded) cooling below M_f can occur without further shape change. Repeated cycles of deformation, followed by heating to give shape recovery, are possible and other types of shape memory behaviour can also be observed.

The application of instrumented indentation to SMAs has expanded in the past decade. One of the main objectives is to obtain local SE and SME characteristics. For this purpose, it is important that a representative volume of material should be interrogated, which usually requires the deformed region to contain at least a handful of grains. As it happens, the grain size of SE alloys is often fairly small, so this requirement may not be too demanding and relatively small indents may be viable, facilitating study of joints and other regions of compositional and microstructural variation in SMA structures. There are also potential advantages in being able to obtain SE characteristics from small samples of simple shape. For example, this facilitates exploration of the effects of varying composition or imposed thermo-mechanical processing conditions. There are, however, various complications associated with the imposition of complex strain fields on SE alloys and interpretation of their indentation response requires care.

The general concept of obtaining bulk mechanical properties from instrumented indentation data is a challenge that has received intensive study over recent years. Of course, the Young's modulus can readily be obtained, from the unloading curve, which can normally be taken to represent purely elastic behaviour. However, this property is usually of limited interest, although in the case of SME alloys the two phases may have significantly different stiffness values, so the phase proportion is relevant to the outcome (Šittner et al., 2014). In addition to the relatively small number of studies aimed at SE and SME characteristics, various attempts have been made to use indentation data to obtain properties of conventional alloys, including quasi-static stress-strain

* Corresponding author.
E-mail address: twc10@cam.ac.uk (T. Clyne).

https://doi.org/10.1016/j.mechmat.2019.04.007
Received 3 October 2018; Received in revised form 7 April 2019
Available online 13 April 2019

relationships, creep characteristics (usually in the steady state regime), the strain rate dependence of plasticity and even fracture characteristics, such as the fracture energy. Most of these attempts have met with limited success and many have been based on seriously flawed assumptions or approximations, mainly concerning treatment of the complex evolving stress and strain fields beneath an indenter (even one with simple geometry, such as a sphere).

The most promising and flexible approach for all of these cases is that of iterative FEM simulation of the indentation process. The concept involved is the simple one of repeatedly changing the values of the material property input parameters until optimum agreement is reached between measured and predicted outcomes. Of course, there are various issues, including choice of the outcomes to monitor, quantification of the "goodness-of-fit" and the need to identify a suitable formulation (constitutive law) describing the behavior concerned. There are also some more subtle challenges, such as how to associate a level of confidence with the set of inferred values, given that there may be a number of alternative combinations giving similar levels of agreement with the experimental outcomes - i.e. the issue of the "uniqueness" of the solution.

Despite these difficulties, progress has been made on developing robust FEM-based methodologies for inferring a number of properties from indentation data - particularly quasi-static plasticity parameters (Guelorget et al., 2007; Dean et al., 2010; Patel and Kalidindi, 2016; Dean and Clyne, 2017; JE Campbell et al., 2018; JE Campbell et al., 2018). Properties exhibiting some sort of time dependence, such as creep and the strain rate sensitivity of plasticity, are rather more complex, particularly in the case of creep, for which behavior in the primary regime tends to dominate the outcomes of indentation experiments (Goodall and Clyne, 2006; Dean et al., 2014). It may be noted that SE behavior can sometimes exhibit (Entemeyer et al., 2006) a dependence on time (i.e. on strain rate), although it is often appropriate to neglect this.

Study of SE behavior using indentation has thus reached an interesting stage. The number of parameters required to characterize the SE response tends to be relatively large, which always makes the procedure more challenging. There is also the complication of whether any conventional plasticity is taking place within the system. (Of course, unlike uniaxial loading, indentation involves large local variations in stress and strain levels, so that inferring what may or may not be happening in different locations requires more sophisticated interpretation of the experimental data.)

There have in fact been a number of studies (Muir Wood and Clyne, 2006; Yan et al., 2007; Muir Wood et al., 2008; Nolan et al., 2010; Farhat et al., 2013; Neupane and Farhat, 2014; Sgambitterra et al., 2015; Sun et al., 2015; Li et al., 2015; Wang et al., 2015; Frost et al., 2015; Perlovich et al., 2016; Kabla and Shilo, 2017) in which the indentation response of materials exhibiting SE have been examined, with many of these (Muir Wood and Clyne, 2006; Nolan et al., 2010; Neupane and Farhat, 2014; Frost et al., 2015; Perlovich et al., 2016) involving numerical (FEM) modeling of the indentation process. Of course, there have also been FEM simulations of the deformation of SE alloys in other types of loading situation (Auricchio and Taylor, 1997; Zhang et al., 2007). Such modeling does require analytical formulation to represent the behavior (i.e. a ``constitutive law"), which, as mentioned above, tends to require a relatively large number of parameters in the case of SE. Nevertheless, some commercial FEM packages, such as ABAQUS, do incorporate standard SE formulations and, at least for most studies in this area, researchers are constrained to use these. This can be particularly problematic for indentation studies of SE, since that formulation does not capture well the unloading response of regions subjected to a range of different strains, which is unavoidable during indentation. This is explained in more detail in §3 below.

In any event, while a number of publications describe work in which SE deformation has been simulated (in relatively complex loading situations, including indentation) by using such packages, there has been little or no systematic work on iterative FEM simulation of indentation in which this mode of deformation is dominant, aimed at convergence between experimental and modeled outcomes. This is regarded as essential if the goal of identifying a robust methodology for obtaining SE parameter values solely from experimental indentation data is to be achieved. The present study is oriented in this direction.

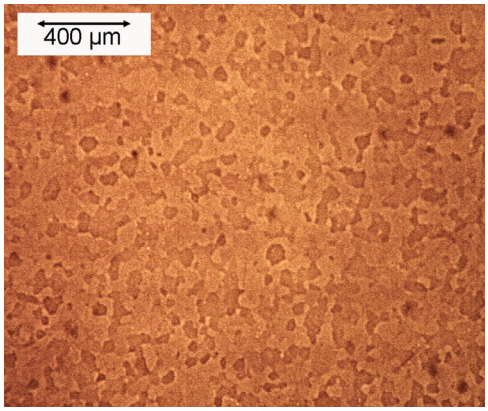

Fig. 1. Optical micrograph of a transverse section of the Ni-Ti rod.

2. Experimental procedures

2.1. Material and microstructure

The present investigation concerns a single type of sample. Rods of Ni-Ti alloy ("Alloy BB") were obtained from Memry Metalle GmbH, specified as having an A_f (austenite finish) temperature of around −10°C. This ensures that they should exhibit superelastic behaviour at room temperature (~20°C). These rods, which had been hot-worked and extruded, had a diameter of 13.3 mm and a length of 300 mm. They were sliced into sections 3 mm in length, mounted and polished (down to 0.25 μm alumina). This produced grain contrast without etching. The grain structure, which can be seen in the optical micrograph of Fig. 1, is approximately equiaxed (in both transverse and axial sections), with a grain size of around 30–50 μm. The composition was investigated using EDX in an SEM, which yielded a value of Ni-49.2at%Ti. This is approximately as expected, although this is not a highly accurate technique and the error on this value may be as high as ± 0.3%.

2.2. X-ray diffraction

XRD was performed with a high-speed Bruker D8 system, using Cu-K_α radiation ($\lambda \sim 0.15418$ nm), with a tube current of 40 mA and a voltage of 40 kV. Diffraction patterns were analysed using the High Score software, involving comparison with patterns from the International Centre for Diffraction Data (ICDD). Scans were in the 2θ range 30–110°, with a step size of 0.05° and a count time at each step of 0.25 s. A typical spectrum is shown in Fig. 2, where it can be seen that (at ambient temperature) the material is composed solely of the B2 austenitic phase.

2.3. Differential scanning calorimetry

DSC was carried out with a Q20 Thermal Analysis instrument, to determine the transition temperatures. Small samples (~5 mg) were cut from the as-received rod and located in high-purity aluminium pans. Runs were performed over a temperature range from between −150 and 100°C, with heating/cooling rates of 10°C min^{-1}. A typical resultant DSC plot is shown in Fig. 3, where it can be seen that the transition temperatures M_s, M_f, A_s and A_f are respectively about −37°C, −78°C, −32°C and −10°C. As expected, these figures show that there

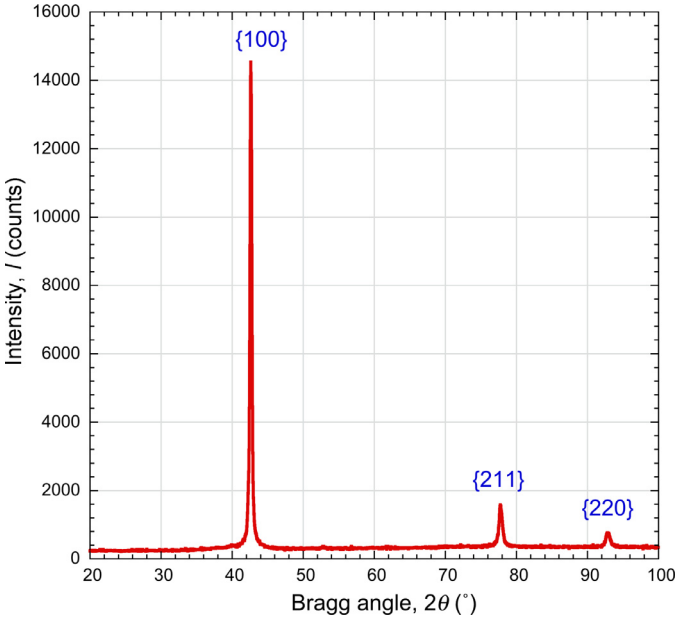

Fig. 2. XRD spectrum from a NiTi sample, showing peaks from only the austenitic (B2) phase, which is cubic (with a lattice parameter of 0.2998 nm).

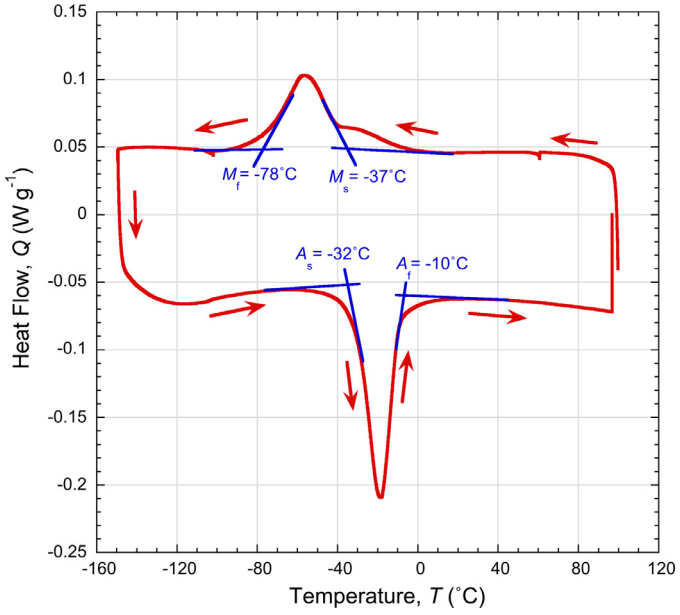

Fig. 3. DSC curves, showing the values obtained for M_s, M_f, A_s and A_f.

is considerable hysteresis in the transitions. They also confirm that the material should be entirely austenitic at room temperature (in the absence of applied stress).

2.4. Uniaxial compression testing

In order to obtain the "correct" superelastic parameter values for this material, samples were subjected to uniaxial compression testing between rigid (hardened steel) platens. Cuboid samples (5 mm × 5 mm × 5 mm) were tested at room temperature (20°C ± 2°C), using MoS_2 lubricant. These were cut with one surface normal to the extrusion axis and testing was carried out both along and transverse to this direction.

Testing was carried out under displacement control (at a rate of 1 mm min^{-1}), using an Instron 3367 screw-driven testing machine, with a load cell having a capacity of 30 kN. The strain rate generated during these tests was thus about $4\,10^{-3}\,s^{-1}$. Tests were carried out up to displacements of about 0.2 mm (~4% strain), so that each test took about 12 s to complete. Several repeat tests were carried out. Both stress and strain levels were converted from nominal to true values, using the standard expressions:

$$\sigma_T = \sigma_N(1 + \varepsilon_N), \quad \varepsilon_T = \ln(1 + \varepsilon_N) \tag{1}$$

with the strains in this case being negative (compressive), so that the true stress has a magnitude lower than the nominal value, while the true strain has a larger magnitude than the nominal strain. This is based on deformation taking place at constant volume. In fact, both conventional elastic deformation and superelastic deformation (occurring via the phase transformation) do involve a volume change, the former being $(1–2\nu)$ times the axial compressive strain and the latter being about −0.4% in this case. These are both very small, so the assumption of constant volume should be acceptable for these purposes.

Displacements were simultaneously measured using two techniques. Firstly, strain gauges (supplied by Omega Engineering Ltd., 0.3 mm grid) were stuck onto the samples, using epoxy adhesive. These had a resolution of about ± 0.1 μm, but had a strain limit of about 2.5%. Secondly, an eddy current gauge (supplied by Micro-Epsilon Ltd was attached to the upper platen and actuated against the lower platen. These had a resolution of about ± 0.25 μm. Only the eddy current gauge could be used for the complete stress-strain loop, but these readings needed to be corrected for the compliance of the loading train over which the gauge was measuring. While this compliance was small, the correction was necessary, since the sample was also quite stiff and the measurements were being made over relatively small displacement ranges. In fact, while the strain gauge readings gave a value for the Young's modulus of the sample (austenitic phase) of ~72 GPa (confirmed by ultrasonic measurements – see below), the eddy current gauge readings lead to a value of ~41 GPa. The compliance correction was ~2.1 μm kN^{-1}. This was subtracted from all of the eddy current gauge readings (bringing the Young's modulus for the initial linear part of the curve up to ~72 GPa).

Representative plots for axial and transverse compression testing are shown in Fig. 4, where it can be seen that there was no systematic differences between the two. A simple numerical average between these

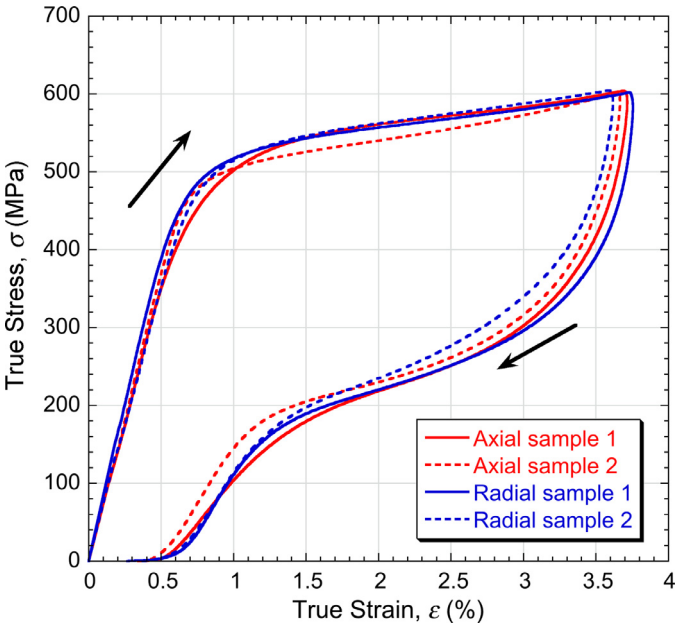

Fig. 4. Stress-strain plots, during loading and unloading at ambient temperature (20°C), for uniaxial compression in axial and radial directions, from testing of 2 samples in each case.

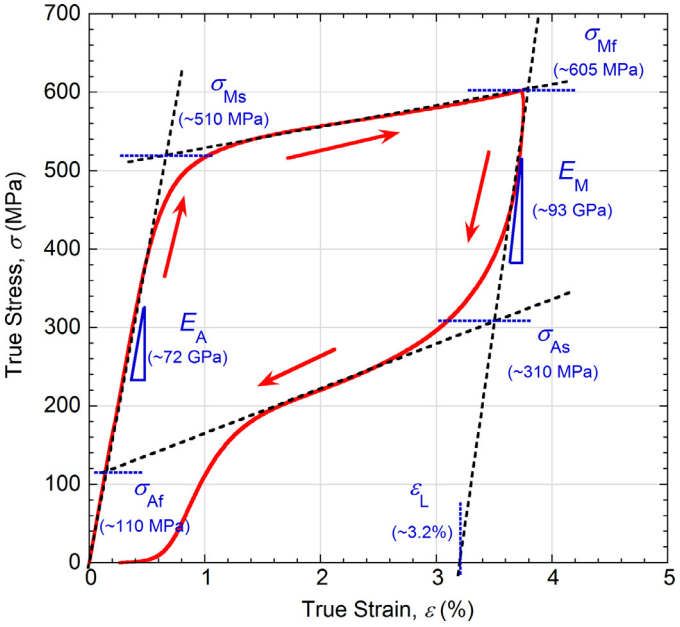

Fig. 5. An averaged experimental stress-strain curve from uniaxial compression, together with fitted values for 7 of the parameters required for input into the ABAQUS FEM model for SE deformation.

runs was taken to be the "target" or "correct" stress-strain curve, with the objective being to infer from indentation data a set of parameter values that captures well this experimental curve. Fig. 5 shows the experimental plot, together with the set of parameter values obtained simply by direct fitting to these data.

The Young's moduli of both austenitic and martensitic phases were measured using a Resonant Frequency Analyser (model system 23, version 6.3.0, supplied by IMCE NV). The specimen was tapped with a small flexible hammer, using an automatic excitation unit. The induced vibration signal was detected with a microphone and the Young's modulus was calculated, using a Poisson ratio value (Otsuka and Ren, 2005; Faiella and Antonucci, 2015) of 0.33. The measurements were performed at room temperature (~20°C) for the austenitic phase. For the martensitic phase, measurable only at low temperatures ($M_f = -78$°C), the sample was dipped into liquid nitrogen (~ −196°C) and quickly tested. The measured moduli were respectively 72 GPa ± 1.0 GPa and 93 GPa ± 1.0 GPa for austenitic and martensitic phases. The eddy current gauge data (Figs. 4 and 5) are consistent with both of these values, after applying the compliance calibration - see above.

2.5. Indentation testing

It is important that a representative volume should be tested, which usually means an assembly of a significant number of grains - preferably more than just a few. In this case, with a grain size of about 30–50 μm, an indent diameter of at least a few hundred microns, and a depth of the order of 15 μm, is likely to be suitable. The indents were therefore created using relatively large (4 mm diameter) sphere of a WC—Co cermet, supplied by Bearing Warehouse Ltd.

This sphere was located in a matching recess in a steel housing, where it was secured by brazing. The set-up is depicted in Fig. 6. Compliance calibration was also needed here, since it is important in work of this type that the displacement data should be obtained under conditions that correspond closely to those being simulated in the model. The compliance was measured by pushing the indenter into a matched recess (about 500 μm deep) in a 5 mm thick plate of alumina, the recess having been created via abrasive rotational honing with the same type of indenter as that used in the tests. After a short bedding-down regime, this gave a linear plot (i.e. constant compliance) and this gradient was subtracted from indentation load-displacement plots. (The contribution to the compliance from the alumina plate itself is considered to be negligible). The compliance measured in this way was ~3.3 μm kN^{-1}.

This calibration coped with the compliance of the housing, including the braze layer between indenter and housing, and also that of the top half of the indenter. However, it did not compensate for the (elastic) deformation of the bottom half of the indenter, which could be significant in the early stages of indentation (when the contact area is small and the stresses and strains in the indenter could be relatively large). This part of the indenter was therefore included in the modelled domain, as shown in Fig. 6.

As with the uniaxial compression testing, these tests were carried out both along and transverse to the extrusion axis of the rod. For the axial testing, indents were made at several radial locations (since it is possible that these experienced different degrees of plastic strain during extrusion, and hence have different textures). For the transverse testing, indentation was carried out along a radial direction. Representative (averaged) load-displacement plots for axial and radial indentation are shown in Fig. 7. No significant differences were found between these two data sets. This is expected, since, as mentioned above, indentation is strongly multi-axial, implying that load-displacement plots obtained from the penetration of a spherical indenter into polycrystalline materials will be independent of the indentation direction. It is also apparent in this figure that, in both cases, there is little or no residual displacement, indicating that the deformation has resulted entirely from (reversible) phase transformations. This is an obvious check to make if the intention is to focus on SE deformation.

2.6. Quantification of the Goodness-of-Fit

The procedure used to quantify the goodness-of-fit between predicted and target indentation outcomes was least squares regression. This is popular for optimising a set of model parameter values, by quantifying the fit between the modelled values of a scalar variable and corresponding expected values (JE Campbell et al., 2018). These are the parameter values that minimise the sum of the squares of the residuals, which are the differences between expected and modelled values of the variable. For the current work, the outcome is a load-displacement plot, the variable is the load (as a function of displacement) and the parameters are those in the selected constitutive law.

More generally, when other material properties are being sought, there are several options concerning the outcomes that might be obtained from experimental load-displacement-time datasets and used as target variables. For example, in the recent work of Burley et al. (Burley et al., 2018), aimed at evaluating a strain rate sensitivity parameter from ballistic indentation experiments, both displacement-time and residual indent shape datasets were used as outcome variables. Having more than one target variable can complicate the convergence procedure, although, in that particular case (with just a single material property parameter to evaluate), simple linear scans in parameter space allowed rapid identification of optimum values.

The sum of the squares of the residuals, S, can be expressed:

$$S = \sum_{i=1}^{N} (P_{i,\mathrm{M}} - P_{i,\mathrm{E}})^2 \tag{2}$$

where $P_{i,\mathrm{M}}$ is the ith value of the modeled displacement (predicted by FEM) and $P_{i,\mathrm{E}}$ is the corresponding experimental (target) value. The value employed for N was around 100. Perfect fit will lead to a value of zero for S. Since S is dimensional, it has units and its magnitude cannot be used to give a universal indication of the quality of the fit. For this purpose, the quantity S_{red}, a "reduced sum of squares" is used, defined by

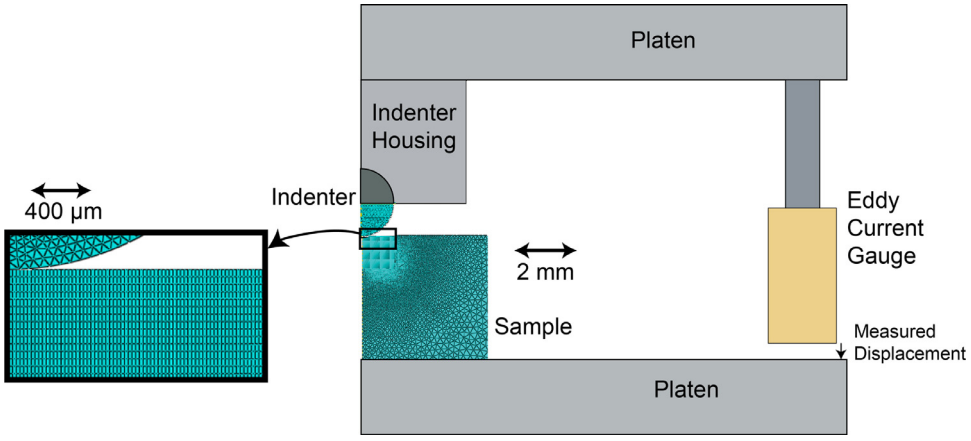

Fig. 6. Schematic of indentation testing set-up, showing the mesh used in the FEM model.

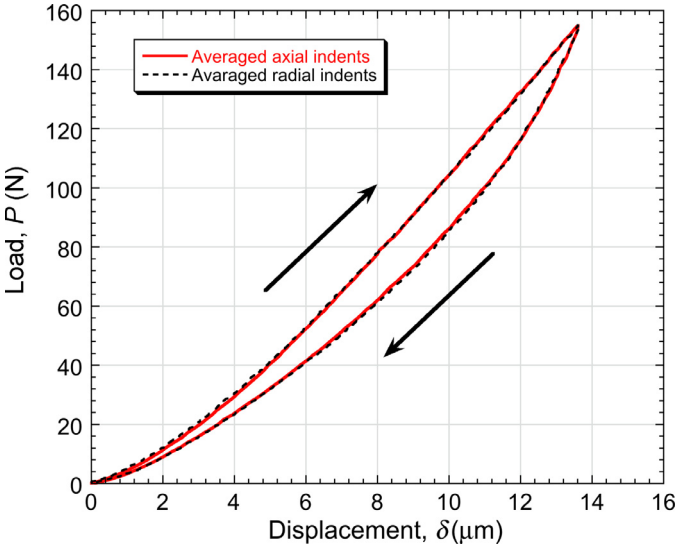

Fig. 7. Representative (averaged) load-displacement plots obtained during indentation in axial and radial directions.

Table 1
Parameter values (for use in the ABAQUS model) obtained from the literature (Faiella and Antonucci, 2015).

Parameter	Symbol	Value
Poisson ratio of Austenite	ν_A	0.33
Poisson ratio of Martensite	ν_M	0.33
Temperature coefficient of phase transition stress (loading)	C_{load}	7 MPa K^{-1}
Temperature coefficient of phase transition stress (unloading)	C_{unload}	7 MPa K^{-1}

Table 2
Elastic constants of the WC−Co cermet indenter.

Parameter	Symbol	Value
Young's modulus	E_{cer}	650 GPa
Poisson ratio	ν_{cer}	0.21

$$S_{red} = \frac{\sum_{i=1}^{N} (P_{i,M} - P_{i,E})^2}{N P_{av,E}^2} \quad (3)$$

where $P_{av,E}$ is the average of the experimentally-measured loads (across the range of displacements being used) and N is the total number of displacement increments. The parameter S_{red} is a positive number, with a value that ranges upwards from 0 (corresponding to perfect fit).

Table 3
Comparison between the SE parameter values obtained by direct fitting to the experimental stress-strain curve (Fig. 5) and via iterative FEM using indentation data.

Parameter	Symbol	Direct fitting to uniaxial data	Inferred from indentation data
Martensite start stress	σ_{Ms}	510 MPa	484 MPa
Martensite finish stress	σ_{Mf}	605 MPa	639 MPa
Transformation strain	ε_L	0.032	0.040
Austenite start stress	σ_{As}	310 MPa	491 MPa
Austenite finish stress	σ_{Af}	110 MPa	238 MPa

A value of S_{red} below about 10^{-3} represents a degree of fit that might generally be regarded as "good". It has been found (JE Campbell et al., 2018) during extraction of plasticity parameters that such values indicate that the material response is being captured well by the set of values concerned. However, it should be recognized that there are some differences with superelasticity. An important point is that the penetration ratio (δ/R) must be kept low ($< \sim 0.75\%$) in order to avoid stimulating conventional plasticity (ie creating peak strains above about 4%). This does generate considerable potential for "compensation" - ie for various sets of input parameter values to give effectively the same (load-displacement) outcome. This is exacerbated by the fact that several (at least about 5) independent parameter values are required to characterize the superelastic stress-strain behaviour. Furthermore, a valuable capability for plasticity is to use the residual indent profile as an additional, or alternative, outcome on which to target the modeling. Of course, this is not an option for superelasticity, which leaves no residual indent. The upshot of these effects is that a value of S_{red} corresponding to "good" fit does not necessarily correspond to a reliable set of parameter values. Also, convergence is likely to be slow - much slower than for plasticity, which is often completed in fewer than 100 iterations.

3. FEM modelling

3.1. Model formulation

An axi-symmetric FEM model for simulation of penetration and withdrawal of a spherical indenter was built within the Abaqus package. Both the indenter and the sample were modelled as deformable bodies and meshed with first order quadrilateral and/or triangular elements. Of course, such modeling allows a check to be made on whether there is any danger of the indenter being plastically deformed.

The volume elements in the model were CAX8R types (linear

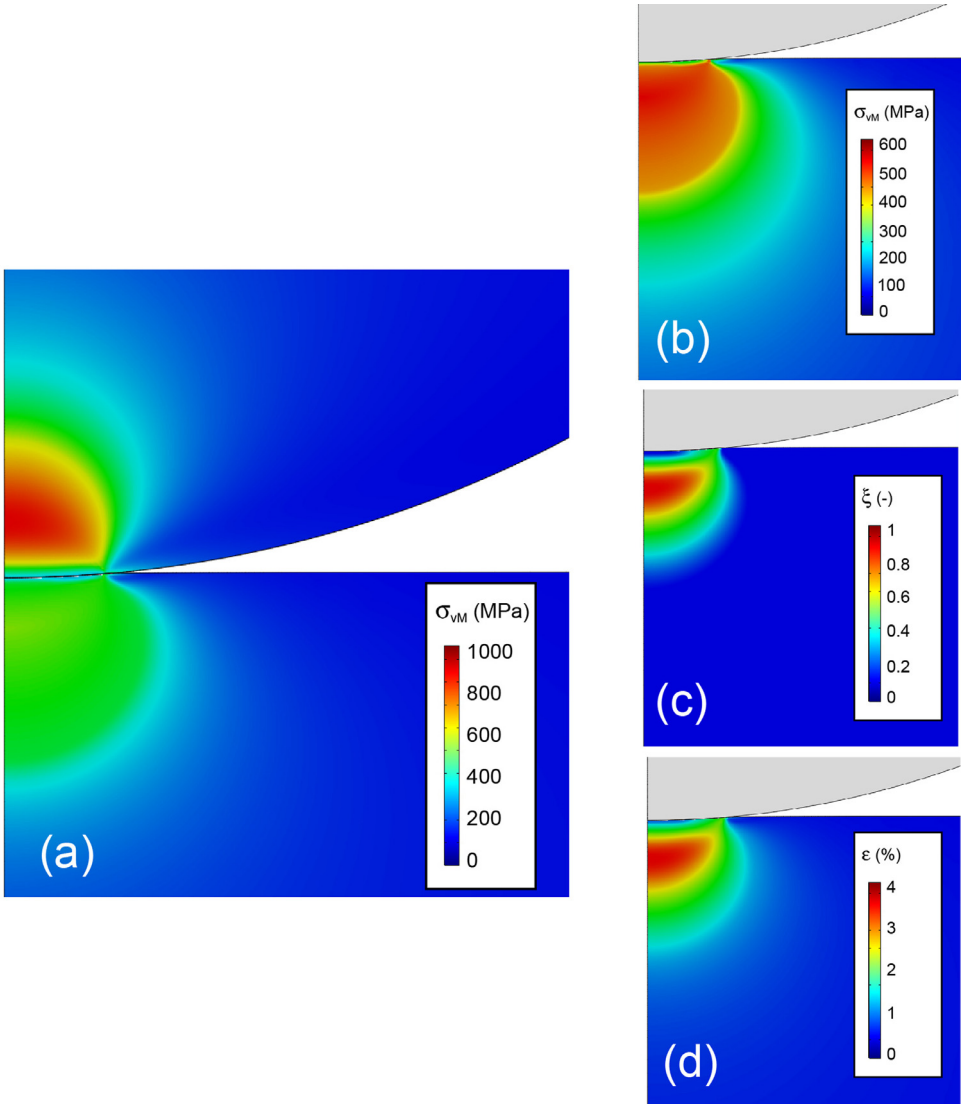

Fig. 8. Outcomes of FEM simulation of the indentation process, obtained using ABAQUS with the set of input parameters shown in Fig. 5, for an applied load of 155 N and a sphere radius of 2 mm. Fields are shown for the (a) von Mises stress for both sample and spherical indenter, (b) von Mises stress for sample (only), (c) local volume fraction transformed to martensite and (d) total strain.

coupled temperature-displacement), with 3146 elements in the sample and 1715 in the indenter. Meshes were refined in regions of the sample close to the indenter. Sensitivity analyses confirmed that the meshes employed were sufficiently fine to achieve convergence, numerical stability and mesh-independent results. The complete sample was included in the simulation, with its rear surface rigidly fixed in place. In modeling the complete sample, contributions to the displacement caused by its elastic deformation (as well as plastic deformation) are fully captured. It was found that, even when the value of the coefficient of friction between sample and indenter was taken to be zero, no frictional sliding occurred during these simulations (so that the value of μ did not affect the outcome).

Assuming that conventional plasticity does not take place and that any tensile-compressive asymmetry can be ignored, the Abaqus user subroutine (UMAT) for superelastic deformation (ABQ_SUPER_ELASTIC_N3D) requires specification of the value of 7 parameters that can be obtained from an experimental stress-strain curve. These 7, together with best fit values, are illustrated in Fig. 5, which shows an experimental plot obtained in the present work. It can be seen that the experimental plot can be simulated with reasonably good fidelity on this basis, although there is a noticeable discrepancy towards the end of unloading, where it is assumed in the ABAQUS formulation that the loading curve is followed below σ_{Mf}, whereas in practice this does not happen. The reason for this is that there is a built-in assumption in the ABAQUS formulation that reversal of the phase transformation is approximately linear with decreasing strain, and is completed before the load has fallen to zero, whereas in practice this is not the case. This discrepancy appears to be quite a significant one, but, short of using a customized FEM package based on a different formulation, it cannot be avoided. It may also be noted that the UMAT routine does in fact introduce a small degree of rounding at the intersections between the linear portions, although this does not change the overall shape of the loading or unloading plots significantly.

The complete set of parameter values to be specified for implementation of the ABAQUS package is shown in Fig. 5 and Tables 1–3. Table 1 shows the values of a further 4 parameters that have been taken from the literature (Faiella and Antonucci, 2015) and Table 2 shows the two elastic constants of the cermet indenter. The values in Table 1 do not, of course, relate to the actual samples being used in the present work, but their magnitude has a relatively small effect on the overall behavior, so ascribing these values to them (which are expected to be of at least approximately the correct magnitude) is considered to be

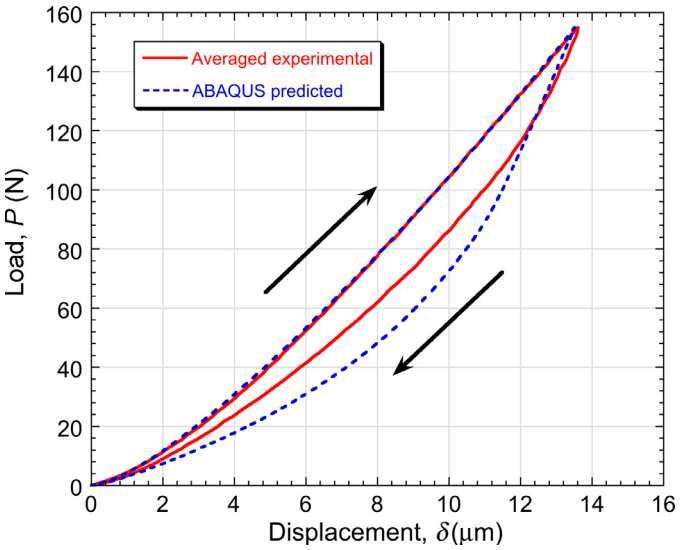

Fig. 9. Comparison between the indentation load-displacement plots obtained experimentally and by FEM simulation (using the best-fit set of parameter values from the uniaxial stress-strain curve).

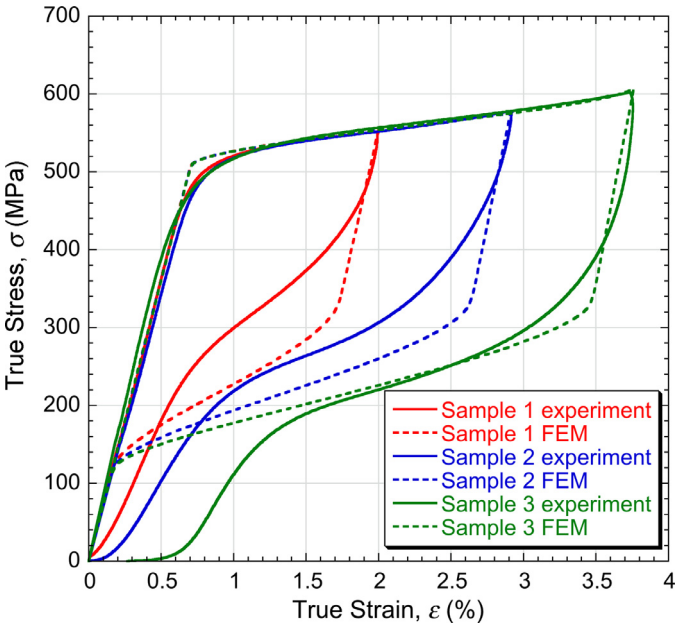

Fig. 10. Comparison between FEM (UMAT) and experimental stress-strain curves for a major loop and two minor loops (transformation to martensite incomplete). The FEM plots correspond to the best-fit set of parameter values from the uniaxial stress-strain curve (Fig. 5).

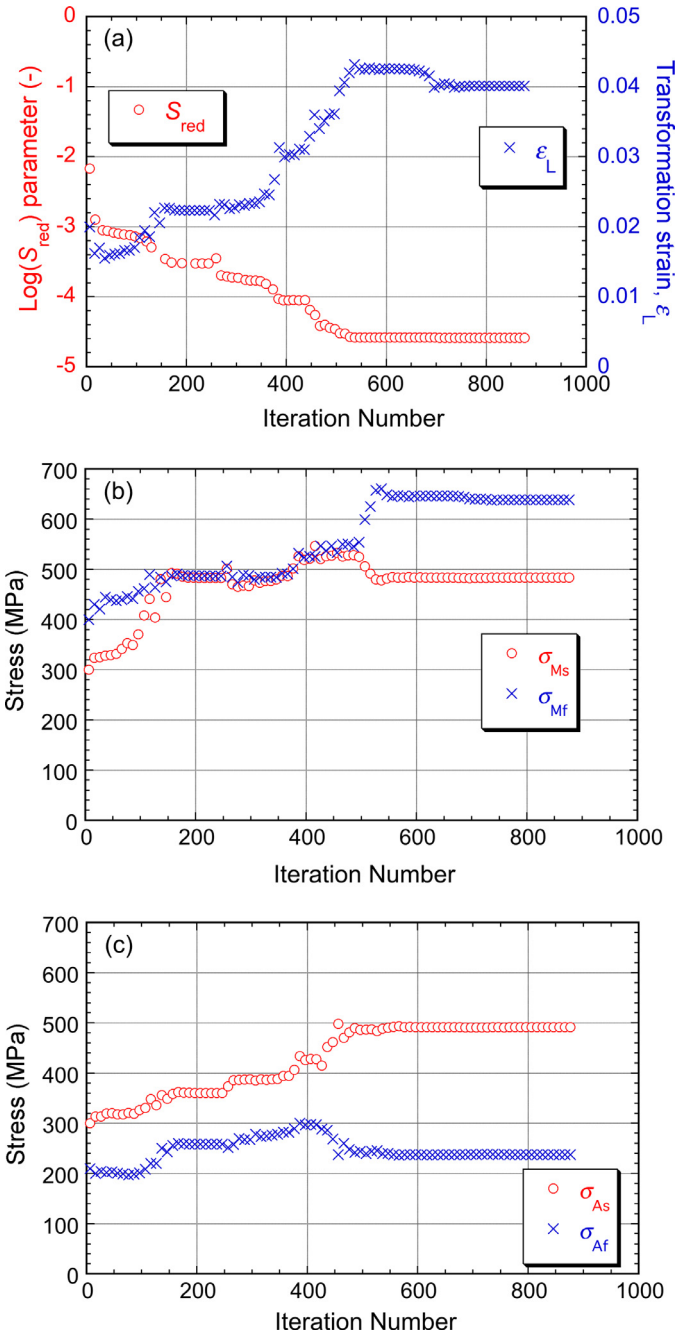

Fig. 11. Nelder-Mead convergence on an optimal (UMAT) parameter set, targetting an indentation load-displacement plot, showing evolution with iteration number of: (a) misfit parameter and transformation strain, (b) martensite start and finish stresses and (c) austenite start and finish stresses.

acceptable here.

3.2. Iterative FEM modelling of indentation

It is a straightforward operation to apply the ABAQUS model to the indentation process, using the best-fit set of parameter values shown in Fig. 5, and hence to obtain a predicted outcome - focused here on the load-displacement relationship, although of course the model can also be used to monitor other outcomes (such as the evolving stress and strain fields, progression of the phase transformation etc.). However, simply checking the consistency in this way is not the main objective of the current exercise, which is to explore the inverse operation of starting with the load-displacement plot and inferring from this the stress-strain relationship - i.e. the values of the SE parameters that define this relationship within the ABAQUS formulation.

This has been done in the current by using the well-known convergence algorithm of Nelder-Mead (JE Campbell et al., 2018; Nelder and Mead, 1965), which is based on study of how the parameter to be minimised (the goodness-of-fit parameter, in this case) behaves in the multi-coordinate space of the parameters to be evaluated (the SE parameters of the material concerned). For a model with m parameters, searching is within an m-dimensional parameter space, within which a *simplex* is defined. This is a *polytope* with $(m + 1)$ vertices (i.e. a triangle in 2-D, a tetrahedron in 3-D etc.). Each vertex corresponds to a particular combination of all of the m parameters in the set and the simplex covers a range of values for all of these. These points can be expressed as vectors (first rank tensors) in parameter space, designated $\boldsymbol{x}_1$, $\boldsymbol{x}_2$,…

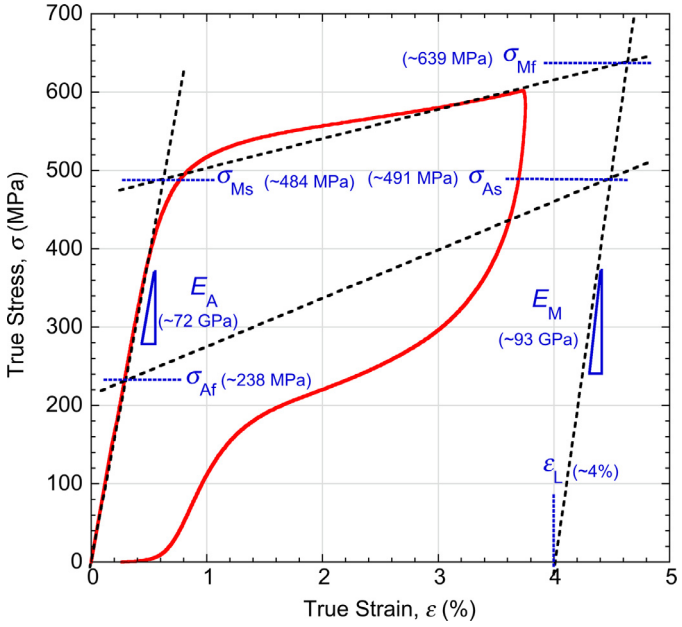

Fig. 12. Comparison between the experimental stress-strain plot (also shown in Fig. 5) and the SE parameter set inferred from the experimental indentation load-displacement plot (shown in Fig. 9), via the Nelder-Mead convergence operation represented in Fig. 11.

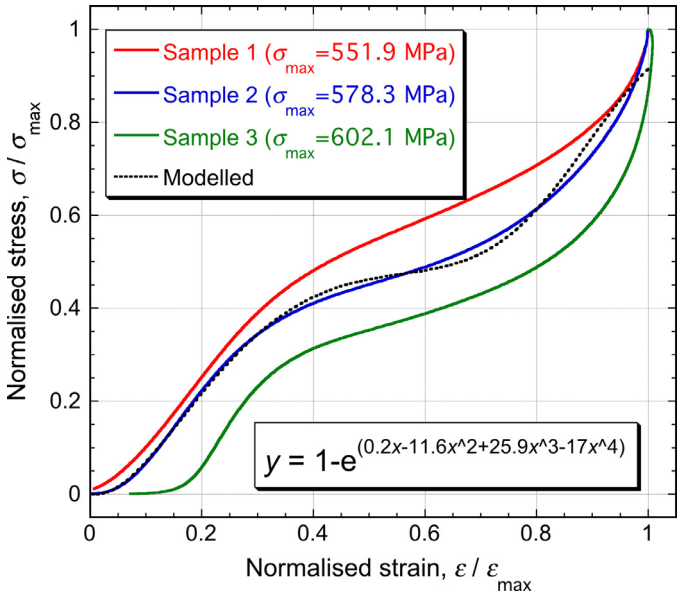

Fig. 13. The unloading parts of the experimental stress-strain curves of Fig. 10, in normalized form, together with an analytical equation that could be used to represent them.

$\boldsymbol{x}_{m+1}$, each of which consists of a set of m parameter values. After each iteration (new FEM simulation), the objective is to "improve" the simplex by replacing the worst vertex (ie the one with the highest value of S) with a better point. The search for this better point is along a line in parameter space defined by the worst point and the centroid of the rest of the simplex, which is the average position of the remaining points (after removal of the worst point).

Firstly, the values in Tables 1 and II were taken to be invariant and excluded from this algorithm. This was also done with the Young's moduli of the two phases in the NiTi alloy, since these are actually well known (and readily measurable). In practical terms, it would commonly be accepted that these could be taken as known or obtainable without using conventional mechanical testing - the objective here, of course, being that of obtaining SE parameter values without doing any such testing.

This leaves a set of 5 parameter values (σ_{Ms}, σ_{Mf}, ε_L, σ_{As} and σ_{Af}) to be optimized in terms of the fit between measured and modeled indentation load-displacement curves. Obtaining convergence in 5-parameter space might be expected to be a relatively slow operation, possibly requiring a large number of iterations of the FEM modeling operation - particularly in view of the relatively shallow penetration - see §2.6.

3.3. Stress, strain and transformation fields during indentation

It is useful to have at least an approximate indication of how the fields of stress and strain, and also progression of the phase transformation, are likely to evolve during the type of indentation being carried out in this work. Some FEM outputs of this type are shown in Fig. 8. It can be seen that the load concerned stimulated complete transformation to the martensitic phase in a region underneath the indenter, generating local strains of about 4%. The (deviatoric) stress levels in this region are about 500–600 MPa. Higher stresses than this are generated in the indenter, but they are well below the levels necessary to induce plastic deformation of the cermet (probably several GPa). It may also be noted that relatively large regions of the sample have undergone only partial transformation to martensite (see below). This is unavoidable during indentation.

4. Estimation of SE parameter values

4.1. Level of agreement using uniaxial parameter values

It is a simple operation to simulate the indentation process, using the set of parameter values fitted to the stress-strain curve, and to compare the predicted load-displacement plot with that obtained experimentally. This comparison is shown in Fig. 9. The level of agreement between the two curves is good for the loading curve, but poor for the unloading curve. This is not surprising, since the fidelity of the ABAQUS UMAT to the stress-strain curve (Fig. 5) is quite poor towards the end of the unloading. Moreover, as mentioned previously, many of the elements that deform during indentation do not fully transform to martensite, as seen in Fig. 8(c), and those will follow minor loops in the stress-strain curve. Fig. 10 shows a comparison between modelled and experimental uniaxial stress-strain curves, with the loading taken to 3 different levels. It can be seen that, for these minor loops, the UMAT formulation gives a very poor representation over virtually the complete unloading range (whereas the major loop, for complete transformation, is poor only towards the end). This is a serious limitation of this formulation for modeling of the indentation of SE materials. It seems clear from this figure that, particularly for simulation of indentation, a formulation is needed that represents these intermediate unloading loops much more closely. Nothing of this type appears to be available at present, at least in terms of routines incorporated into commercial FEM packages.

4.2. Outcome of the convergence operation

While the appearance of Fig. 10 is far from encouraging, a Nelder-Mead convergence operation was carried out, using the averaged experimental load-displacement plot as a target. The outcome is shown in Fig. 11. Successful convergence was achieved (after a relatively large number of iterations) and the resultant values of the SE parameter set are shown in this figure, presented in Table 3 and also plotted as a stress-strain curve in Fig. 12. It can immediately be seen from Fig. 12 that, while the agreement is fairly good for the loading curve (except in terms of the peak strain), it is poor for the whole of the unloading curve. It seems clear that this is due to the poor fidelity between the actual

unloading curves experienced by the various volume elements deformed during the indentation operation and the way that these are represented in the UMAT routine for their simulation.

Furthermore, the nature of the discrepancy can be at least qualitatively understood. During unloading, at a given strain, the actual load carried by most individual volume elements is higher than that being simulated, at least until the strain becomes very small (Fig. 10). When constrained by the UMAT representation, the convergence operation leads to compensation for this by raising σ_{As} and σ_{Af} (Fig. 12).

4.3. Improved representation of the unloading curves

It seems clear that what is required here is a more realistic formulation for the unloading curves. From a mathematical point of view, this should not be a major challenge. For example, a "Dose-Response" expression (commonly used in biological investigations) of the following type (4-stage with zero background)

$$y = 1 - exp(Ax + Bx^2 + Cx^3 + Dx^4) \quad (4)$$

can exhibit a similar shape to those of typical unloading curves. When the experimental unloading curves are normalised, they do not collapse accurately onto a single master curve, but they are not so far from doing this. This is illustrated by the plots shown in Fig. 13, in which the unloading data from Fig. 10 have been normalised and are compared with the curve obtained using Eqn. (4) with a particular set of coefficient values (shown in the figure). This might be suitable, or at least be better than the UMAT formulation, using a pre-determined set of coefficient values in this way. Furthermore, since there seems to be a systematic trend, it may be possible to obtain a better fit than this by establishing an analytical relationship between the maximum load or strain (ie the fractional distance along the part of the loading curve where the phase transformation is occurring) and the values of the coefficients in Eqn. (4). Of course, such a formulation would need to be integrated into a suitable FEM model, but this should be relatively straightforward, at least in principle.

5. Conclusions

The following conclusions can be drawn from this work:

(a) Uniaxial compression and (spherical) indentation experiments have been carried out on a commercially-available NiTi alloy that exhibits superelastic behaviour at room temperature. The uniaxial stress-strain loop is of the type expected and it has been represented here via a set of parameter values that define a series of linear sections. Such a set of parameter values can be used within an ABAQUS FEM package (with the UMAT formulation). It is noted that this representation is not a very accurate one for the unloading part of the curve, particularly if the maximum strain experienced is significantly below that corresponding to full transformation of the austenite to martensite.

(b) The objective of the work is to develop a methodology for obtaining the superelastic (stress-strain) characteristics solely from an indentation experiment. The approach used, which is already well-developed for plasticity, involves iterative FEM simulation of the indentation process, initially using trial values for the parameters involved in the constitutive law and converging on best fit values by seeking to optimise the agreement between experimental and modelled outcomes (load-displacement plots in this case). This operation has been carried out and values obtained.

(c) The level of agreement between the experimental stress-strain plot and the one obtained via an indentation experiment is good for the loading part of the curve, but poor for the unloading part. This is attributed to limitations of the formulation for the unloading in the standard set of parameter values (in the UMAT routine available in ABAQUS), as noted above.

(d) It seems clear that, certainly in order for the indentation route to be viable, and perhaps more generally, an improved representation is required for the unloading part of superelastic stress-strain curves. An analytical formulation that could form the basis for this is put forward here.

Acknowledgements

This work is supported by CNPq (grant 202250/2014-8) (Brazilian National Council for Research) and by the EPSRC (grants EP/I038691/1 and EP/K503757/1).

In compliance with current EPSRC requirements, input data for the modeling described in this paper, including meshing and boundary condition specifications, are available at the following URL: www.ccg.msm.cam.ac.uk/publications/resources. These files can be downloaded and used in FEM models.

Supplementary materials

Supplementary material associated with this article can be found, in the online version, at doi:10.1016/j.mechmat.2019.04.007.

References

Auricchio, F, Taylor, RL., 1997. Shape-memory alloys: modelling and numerical simulations of the finite-strain superelastic behavior. Comput. Methods Appl. Mech. Eng. 143, 175–194.
Burley, M, Campbell, JE, Dean, J, Clyne, TW, 2018. Johnson-Cook parameter evaluation from ballistic impact data via iterative FEM modelling. Int. J. Impact Eng. 112, 180–192.
Campbell, JE, Kalfhaus, T, Vassen, R, Thompson, RP, Dean, J, Clyne, TW, 2018. Mechanical properties of sprayed overlayers on superalloy substrates, obtained via indentation testing. Acta Materialia 154, 237–245.
Campbell, JE, Thompson, RP, Dean, J, Clyne, TW, 2018. Experimental and computational issues for automated extraction of plasticity parameters from spherical indentation. Mech. Mater. 124, 118–131.
Dean, J, Campbell, J, Aldrich-Smith, G, Clyne, TW, 2014. A critical assessment of the "Stable Indenter Velocity" method for obtaining the creep stress exponent from indentation data. Acta Materialia 80, 56–66.
Dean, J, Clyne, TW., 2017. Extraction of plasticity parameters from a single test using a spherical indenter and FEM modelling. Mech. Mater. 105, 112–122.
Dean, J, Wheeler, JM, Clyne, TW, 2010. Use of quasi-static nanoindentation data to obtain stress-strain characteristics for metallic materials. Acta Materialia 58, 3613–3623.
Entemeyer, D, Patoor, E, Eberhardt, A, Barveiller, M, 2006. Strain rate sensitivity in superelasticity. Int. J. Plast. 16, 1269–1288.
Faiella, G, Antonucci, V., 2015. Chapter 3 - experimental characterization of shape memory alloys. editor In: Concilio, LL (Ed.), Shape Memory Alloy Engineering. Butterworth-Heinemann, Boston, pp. 57–77.
Farhat, Z, Jarjoura, G, Shahirnia, M, 2013. Dent resistance and effect of indentation loading rate on superelastic TiNi alloy. Metall. Mater. Trans. A 44A, 3544–3551.
Frost, M, Kruisova, A, Shanel, V, Sedlak, P, Hausild, P, Kabla, M, et al., 2015. Characterization of superelastic NiTi alloys by nanoindentation: experiments and simulations. Acta Physica Polonica A 128, 664–669.
Goodall, R, Clyne, TW., 2006. A critical appraisal of the extraction of creep parameters from nanoindentation data obtained at room temperature. Acta Materialia 54, 5489–5499.
Guelorget, B, Francois, M, Liu, C, Lu, J, 2007. Extracting the plastic properties of metal materials from microindentation tests: experimental comparison of recently published methods. J. Mater. Res. 22, 1512–1519.
Kabla, M, Shilo, D., 2017. Characterization of NiTi superelastic properties by nano-dynamic modulus analysis and nanoindentation. Funct. Mater. Lett. 10, 1650071.
Li, P, Karaca, HE, Cheng, Y-T, 2015. Spherical indentation of NiTi-based shape memory alloys. J. Alloys Comp. 651, 724–730.
Muir Wood, AJ, Clyne, TW, 2006. Measurement and modelling of the nanoindentation response of shape memory alloys. Acta Materialia 54, 5607–5615.
Muir Wood, AJ, Sanjabi, S, Fu, YQ, Barber, ZH, Clyne, TW, 2008. Nanoindentation of binary and ternary Ni–Ti-based shape memory alloy thin film. Surf. Coat. Technol. 202, 3115–3120.
Nelder, JA, Mead, R., 1965. A simplex method for function minimization. Comput. J. 7, 308–313.
Neupane, R, Farhat, Z., 2014. Prediction of Indentation Behavior of Superelastic TiNi. Metall. Mater. Trans. A 45A, 4350–4360.
Nolan, JM, Hartl, DJ, Lagoudas, DC, Grummon, DS, 2010. 3-D finite element analysis of indentation recovery due to the shape memory effect. In: Ounaies, Z, Li, J (Eds.), Behavior and Mechanics of Multifunctional Materials and Composites. Spie-Int Soc Optical Engineering, Bellingham, pp. 2010.
Otsuka, K, Ren, X., 2005. Physical metallurgy of Ti–Ni-based shape memory alloys.

Progress Mater. Sci. 50, 511–678.
Patel, DK, Kalidindi, SR., 2016. Correlation of spherical nanoindentation stress-strain curves to simple compression stress-strain curves for elastic-plastic isotropic materials using finite element models. Acta Materialia 112, 295–302.
Perlovich, Y, Isaenkova, M, Zhuk, D, Krymskaya, O, 2016. Accessing mechanical properties of superelastic materials from microindentation data by computer modelling. In: Proceedings of 2016 6th International Workshop on Computer Science and Engineering.
Saburi, T, 1998. Ti-Ni *shape memory alloys*. editors. In: Otsuka, K, Wayman, CM (Eds.), Shape Memory Materials. CUP, Cambridge:, pp. 49–96.
Sgambitterra, E, Maletta, C, Furgiuele, F, 2015. Temperature dependent local phase transformation in shape memory alloys by nanoindentation. Scripta Materialia 101, 64–67.
Šittner, P, Heller, L, Pilch, J, Curfs, C, Alonso, T, Favier, D, 2014. Young's modulus of austenite and martensite phases in superelastic NiTi wires. J. Mater. Eng. Perform. 23, 2303–2314.
Sun, Y, Zhao, G, Yang, F, 2015. Effect of electric current on nanoindentation of superelastic NiTi alloy. Exp. Mech. 55, 1503–1509.
Van Humbeeck, J, Stalmans, R, 2002. Shape memory alloys, types and functionalities. editor In: Schwartz, M (Ed.), Encyclopaedia of SMART MATERIALS. John Wiley and Sons, Inc., pp. 951–964.
Van Humbeeck, J., 2001. The martensitic transformation. In: Shaller, R, Fantozzi, G, Gremaud, G (Eds.), Mechanical Spectroscopy. Trans Tech Publications, pp. 382–415.
Wang, LQ, Wang, C, Lu, WJ, Zhang, D, 2015. Superelasticity of NiTi-Nb metallurgical bonding via nanoindentation observation. Mater. Lett. 161, 255–258.
Yan, W, Sun, Q, Feng, X-Q, Qian, L, 2007. Analysis of spherical indentation of superelastic shape memory alloys. Int. J. Solids Struct. 44, 1–17.
Zhang, Y, Cheng, Y-T, Grummon, DS, 2007. Finite element modeling of indentation-induced superelastic effect using a three-dimensional constitutive model for shape memory materials with plasticity. J. Appl. Phys. 101, 053507.